Antitumor Efficacy of 34.5ENVE: A Transcriptionally Retargeted and "Vstat120"-expressing Oncolytic Virus

Ji Young Yoo[1], Amy Haseley[1], Anna Bratasz[2,3], E Antonio Chiocca[1], Jianying Zhang[4], Kimerly Powell[2,3] and Balveen Kaur[1]

[1]Department of Neurological Surgery, Dardinger Laboratory for Neuro-oncology and Neurosciences, The Ohio State University Medical Center, Columbus, Ohio, USA; [2]Small Animal Imaging Shared Resources, The Ohio State University Medical Center, Columbus, Ohio, USA; [3]Department of Biomedical Informatics, James Comprehensive Cancer Center, Columbus, Ohio, USA; [4]Center for Biostatistics, The Ohio State University Medical Center, Columbus, Ohio, USA

Here, we describe the construction and testing of a novel herpes simplex virus type 1 (HSV-1) derived oncolytic virus (OV): 34.5ENVE (viral ICP**34.5** **E**xpressed by **N**estin promotor and **V**stat120 **E**xpressing), for the treatment of cancer. This virus showed significant glioma-specific killing and antiangiogenic effects *in vitro* and *in vivo*. Treatment of subcutaneous and intracranial glioma-bearing mice with 34.5ENVE showed a significant increase in median survival of mice in four different glioma models. Histology and dynamic contrast-enhanced magnetic resonance imaging (DCE-MRI) revealed reduced microvessel density (MVD) and increased tumoral necrosis in 34.5ENVE-treated tumor tissue compared to control OV-treated tumor tissue. Collectively, these results describe the construction, efficacy, and impact on tumor microenvironment of a transcriptionally driven OV armed with Vstat120 gene expression. These preclinical results will facilitate future clinical testing of 34.5ENVE.

Received 24 February 2011; accepted 30 August 2011; published online 25 October 2011. doi:10.1038/mt.2011.208

INTRODUCTION

The poor prognosis associated with Glioblastoma multiforme underscores the urgent need to seek out novel strategies to improve patient outcome.[1] Oncolytic virus (OV) therapy is one of such strategies, as it utilizes viruses with a propensity to replicate and destroy cancer cells as an antineoplastic agent. First generation OVs have been tested in patients and have been proven safe, yet have revealed limited efficacy.[2–4]

We have previously created and tested the therapeutic efficacy of a first generation OV armed with the antiangiogenic gene *Vstat120* (RAMBO).[5] While this virus showed significant antitumor efficacy compared to control rHSVQ1, single treatment of mice with established intracranial tumors resulted in only 20% of the mice showing a complete response. It is likely that the highly attenuated rHSVQ1 viral backbone of RAMBO limited oncolysis and antitumor efficacy. Several innovative approaches are currently under investigation to enhance OV therapeutic efficacy, and transcriptional retargeting of viral replication is one of such exciting approaches.[6–8] rQnestin34.5 is one such virus which is enhanced by transcriptional retargeting as it expresses viral ICP34.5 under the regulation of a glioma-specific nestin promotor in an ICP34.5 deleted viral backbone.[7,9–11] This virus has shown significant antitumor efficacy against glioma and neuroblastoma tumors.[9,11] Thus, we hypothesized that incorporation of Vstat120 within the rQnestin34.5 backbone would show enhanced antitumor efficacy compared to RAMBO or rQnestin34.5.

Based on these results we engineered and tested the therapeutic efficacy of arming rQnestin34.5 with the antiangiogenic gene *Vstat120*. Here, we describe the construction of a novel OV, 34.5ENVE (viral ICP**34.5** **E**xpressed by **N**estin promotor and **V**stat120 **E**xpressing). This virus showed significant glioma-specific killing and antiangiogenic effects *in vitro* and *in vivo*. In addition to the nestin driven specificity of 34.5ENVE, we also observed a highly significant increase in antitumor efficacy, even at a single intratumoral injection, in intracranial glioma-bearing mice. Dynamic contrast-enhanced magnetic resonance imaging (DCE-MRI) revealed increased blood–brain barrier permeability (increased K^{trans}) in tumors treated with OV compared to control phosphate-buffered saline (PBS)-treated tumors indicating OV-mediated increased blood–brain barrier disruption. Additionally, both histology and calculated DCE-MRI parameters revealed a significant increase in necrotic areas in 34.5ENVE-treated compare to rQnestin34.5-treated tumors.

RESULTS

Generation and characterization of recombinant 34.5ENVE

34.5ENVE, an OV-expressing Vstat120 within the backbone of rQnestin34.5, was engineered using HSVQuik technology as described.[12] **Figure 1a** shows the genetic structures of wild-type herpes simplex virus type 1 (HSV-1) and 34.5ENVE along with the first and second generation OVs used in this study. rHSVQ1 is a first

The first two authors contributed equally to this work.

Correspondence: *Balveen Kaur, Department of Neurological Surgery, Dardinger Laboratory for Neuro-oncology and Neurosciences, The Ohio State University, 385-D OSUCCC, 410 West 12th Avenue, Columbus, Ohio 43210, USA. E-mail address: Balveen.Kaur@osumc.edu*

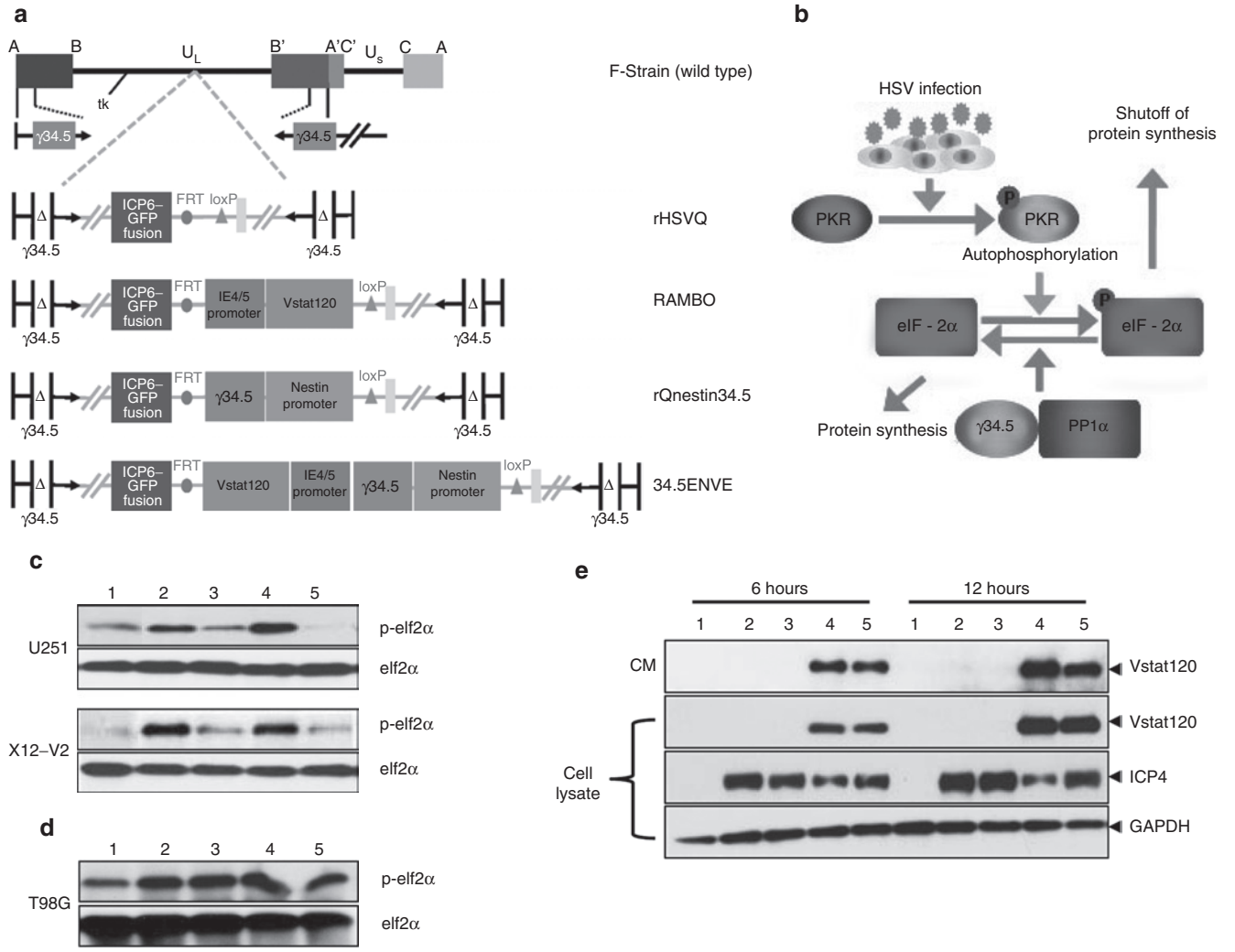

Figure 1 Structure and characterization of 34.5ENVE. (**a**) Genetic map of wild-type herpes simplex virus type 1 (HSV-1), and the various oncolytic viruses (OVs) used in this study. (**b**) Activation of PKR upon OV infection causes phosphorylation of eIF2α, and subsequent shutoff of protein synthesis. Viral ICP34.5 activates protein phosphatase 1α, to reverse phosphorylation of eIF2α and the subsequent protein translation. (**c**) Western blot analysis of phosphorylated and total eIF2α in high nestin-expressing U251 and X12-V2 glioma cells treated with phosphate-buffered saline (PBS) (lane 1) or infected with rHSVQ1 (lane 2), rQnestin34.5 (lane 3), RAMBO (lane 4), or 34.5ENVE (lane 5) [multiplicity of infection (MOI) = 0.1], 24 hours postinfection. (**d**) Western blot analysis of phosphorylated and total eIF2α in low nestin-expressing T98G glioma cells treated similarly (MOI = 0.1), 24 hours postinfection. (**e**) Western blot analysis of U251 glioma cells treated with PBS (lane 1), rHSVQ1 (lane 2), rQnestin34.5 (lane 3), RAMBO (lane 4), or 34.5ENVE (lane 5) at an MOI = 0.1. The cells were harvested at 6 and 12 hours postinfection and analyzed for expression of secreted and cellular Vstat120 and ICP4. Note the presence of Vstat120 in cells infected with RAMBO and 34.5ENVE.

generation OV deleted for both copies of ICP34.5 and disrupted for ICP6; rQnestin34.5 is a transcriptionally driven OV, expressing ICP34.5 under the control of the glioma-specific nestin promotor in an rHSVQ1 backbone; RAMBO is a Vstat120-expressing OV within the rHSVQ1 backbone; and 34.5ENVE expresses Vstat120 within the rQnestin34.5 viral backbone.[5,9] **Figure 1b** shows a schematic of the PKR-activated cellular defense response and the role of viral ICP34.5 in this process. Activation of cellular PKR, postviral infection, results in phosphorylation of cellular eIF2α and subsequent shut down of protein synthesis.[13] Viral ICP34.5 activates cellular phosphatases, leading to dephosphorylation of eIF2α thus permitting protein synthesis and viral replication. The phosphorylation state of cellular eIF2α in infected cells was evaluated to investigate the expression of functional ICP34.5. As expected, **Figure 1c** demonstrates increased phosphorylation of eIF2α (P-eiF2α) in glioma cells infected with control ICP34.5 deleted OVs (rHSVQ1 or RAMBO). Reduced P-eiF2α in glioma cells infected with 34.5ENVE or rQnestin34.5 was evident in cells positive for nestin expression (U251 and X12-V2), but not in glioma cells with low nestin expression (T98G) (**Figure 1c,d**). The ability of 34.5ENVE to produce Vstat120 was evaluated in U251 glioma cells infected with control (rHSVQ1 or rQnestin34.5) or Vstat120 expressing (RAMBO or 34.5ENVE) OV. Western blot analysis revealed efficient production and secretion of Vstat120 from glioma cells infected with RAMBO or 34.5ENVE (**Figure 1e**).

Oncolysis of 34.5ENVE in nestin-expressing glioma cells

Viral ICP34.5 is driven by the nestin promotor in rQnestin34.5 and it has been shown to have increased virus replication compared

to rHSVQ1 in nestin-expressing glioma and neuroblastoma cells, but not in low nestin-expressing cells.[9,11] To test whether insertion of the *Vstat120* gene expression cassette alters the specificity of rQnestin34.5 replication, we compared the viral replication of rQnestin34.5 and 34.5ENVE in twelve different glioma cell lines and primary normal cells. As glioma cells are varyingly susceptible to virus infection, we normalized the fold increase in replication of 34.5ENVE and rQnestin34.5 to ICP34.5 deleted rHSVQ1. **Figure 2a** shows the scatter plot in Log2 function for the fold change in replication of rQnestin34.5 and 34.5ENVE relative to rHSVQ1 in 12 glioma and normal cell lines. There was a statistically significant positive correlation between the replication of rQnestin34.5 and 34.5ENVE ($r = 0.95091$, $P < 0.0001$), suggesting that Vstat120 expression did not alter specificity of rQnestin34.5 replication in different cell lines. To determine whether 34.5ENVE retained glioma cell-specific oncolysis, we compared the cytotoxic ability of the four different viruses in cells with high and low nestin expression (**Supplementary Figure S1**). Consistent with nestin promotor enhanced virus replication, both rQnestin34.5 and 34.5ENVE showed statistically significant increased cytotoxicity

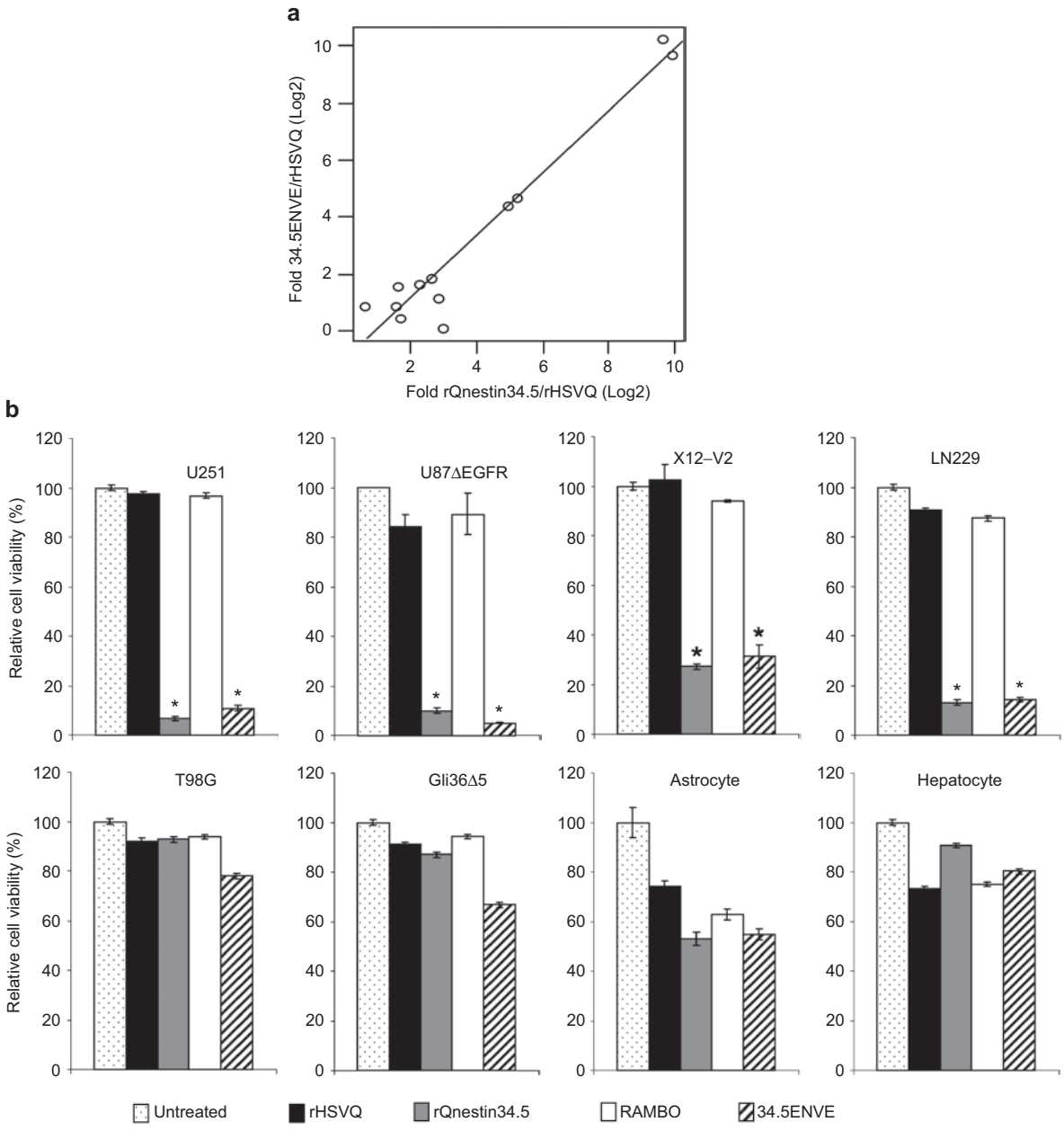

Figure 2 Increased virus replication and cytopathic effect of 34.5ENVE in high nestin-expressing cells. Twelve different cell lines (glioma and normal) were infected with rHSVQ1, rQnestin34.5, or 34.5ENVE [multiplicity of infection (MOI) = 0.001]. Seventy-two hours postinfection the amount of rHSVQ1, rQnestin34.5, and 34.5ENVE in each cell line was evaluated by plaque assay. (**a**) Scatter plot of relative virus yield of Log2 fold increase in 34.5ENVE to rQnestin34.5 relative to rHSVQ1 in each cell line. Each dot represents 1 of the 12 glioma/primary cells evaluated. (**b,c**) Quantification of cell viability in the indicated cells infected with rHSVQ1, rQnestin34.5, RAMBO, or 34.5ENVE (MOI = 0.05) relative to phosphate-buffered saline (PBS) 3 days postinfection.

(relative to rHSVQ1) in nestin-expressing cells (U251, U87ΔEGFR, LN229, and X12-V2) but not in cells with low or negative nestin expression (T98G, Gli36Δ5, human normal astrocyte, and human normal hepatocyte) (**Figure 2b,c**).

34.5ENVE inhibits endothelial cell migration and tube formation *in vitro* and *in vivo*

Next, we tested the effect of 34.5ENVE on endothelial cell migration and tube formation *in vitro*. To investigate this, we evaluated tube formation ability of endothelial cells cultured with conditioned media (CM) derived from OV-infected glioma cells (HSV-1 neutralizing antibody was added to the CM to avoid secondary infection of endothelial cells by contaminating virus particles). **Figure 3a** shows representative images of the formation of elongated tube-like structures in endothelial cells treated with CM derived from U251 cells treated with PBS, or the indicated virus; structured tube number/view is quantified in **Figure 3b**. Note the significant reduction in the number of tubes obtained from the cells treated with 34.5ENVE and RAMBO compared to rHSVQ1 or rQnestin34.5-infected cells ($P < 0.001$). We also investigated the effects of 34.5ENVE on the migration of human dermal microvascular endothelial cells (HDMECs) in a transwell chamber. Quantitative analysis showed that CM collected from U251 cells infected with 34.5ENVE or RAMBO significantly reduced the migration of endothelial cells by 33 and 34.1%, respectively, relative to rHSVQ1 (**Figure 3c**). Collectively, these findings demonstrate that 34.5ENVE effectively inhibits endothelial cell tube formation and migration *in vitro*. To determine the

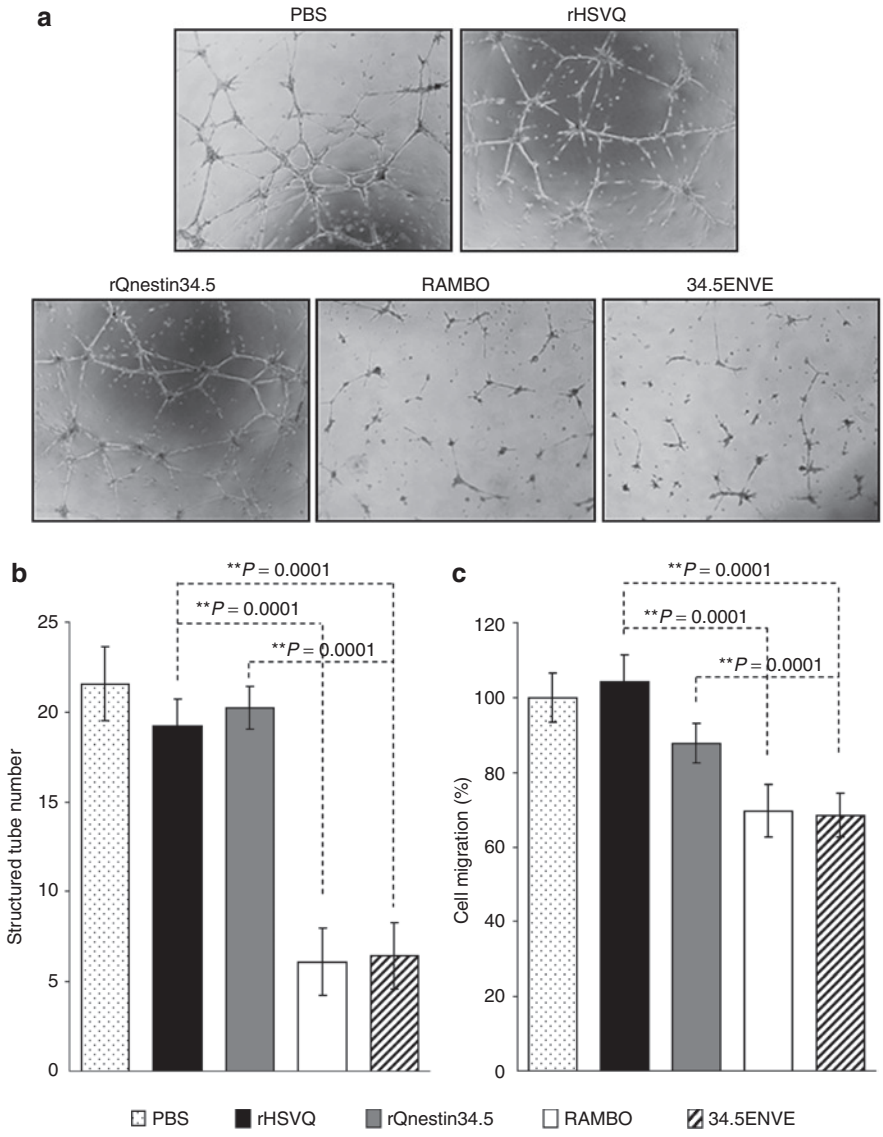

Figure 3 Antiangiogenic effect of 34.5ENVE *in vitro*. (**a**) Images of endothelial cell tube formation after being cultured on Matrigel. Endothelial cells were incubated with conditioned medium (CM) derived from U251 cells infected with the indicated virus or phosphate-buffered saline (PBS). (**b**) Quantification of the average number of tubes/view field ($n = 4$/group) observed above. (**c**) Inhibition of endothelial cell migration: human dermal microvascular endothelial cells (HDMECs) were incubated with CM derived from U251 cells treated with PBS, or the indicated virus. Cells were plated in the upper chamber of transwell and allowed to migrate toward CM used as a chemoattractant in the bottom chamber. The migrated cells on the bottom side of the filter were quantified as described ($n = 4$/group).[26] Data are presented as mean ± SEM of number of cells/view field.

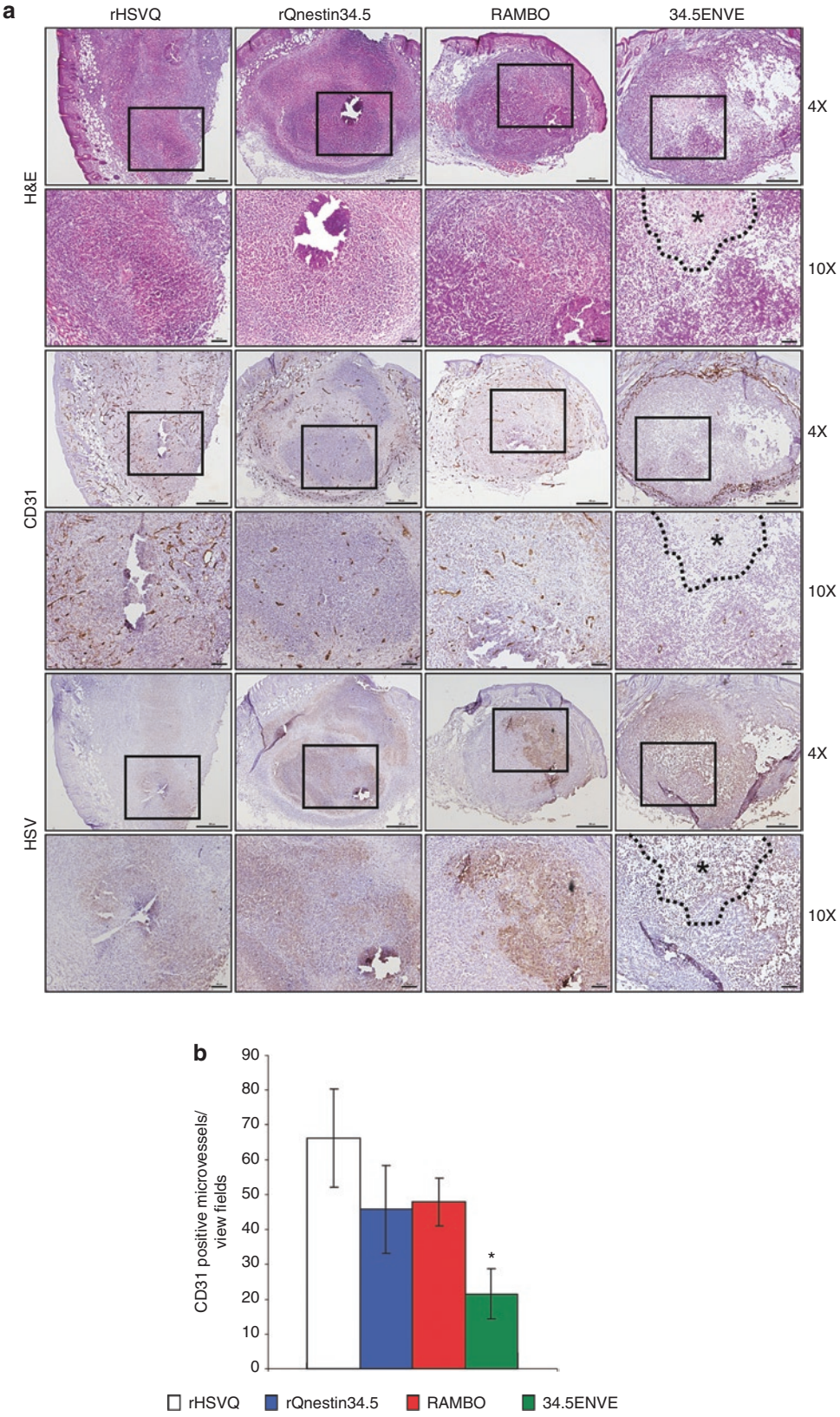

Figure 4 Reduced angiogenesis in tumors treated with 34.5ENVE. (**a**) Representative images of immunohistochemistry for hematoxylin and eosin (H&E), CD31, and HSV-1 staining of adjacent tumor sections treated with phosphate-buffered saline (PBS), or the indicated virus. Necrotic area is marked by asterisks and black dotted lines. (**b**) Quantification of microvessel density (MVD) in tumors treated with PBS, or the indicated virus. Data shown are mean MVD ± SEM for each group (n = 6 sections/tumor and n = 3 tumors/group). All bars are 100 µm for ×10 magnification images and 500 µm for ×4 images, respectively.

impact of 34.5ENVE on tumoral angiogenesis *in vivo*, we compared microvessel density (MVD) in a U251T3 subcutaneous tumor xenograft model as described by Weidner *et al.*[14] **Figure 4a** shows representative images of adjacent tumor sections stained with hematoxylin and eosin, anti-HSV-1, and anti-CD31 antibodies at high and low magnification. **Figure 4b** shows quantification of $CD31^+$ blood vessels in viable tumor tissue adjacent to HSV-1 positive staining tumor area. Quantification revealed 3.5-, 2.1-, and 1.8-fold reduction in MVD in tumors treated with 34.5ENVE compared to rHSVQ1, rQnestin34.5, or RAMBO, respectively (P = 0.0001, 0.0002, and 0.0033, respectively).

Antitumor effects of 34.5ENVE *in vivo*

We next investigated the antitumor effects of 34.5ENVE *in vivo* in four different glioma models. Mice with subcutaneous tumors (U251T3 glioma cells) were treated with PBS, rQnestin34.5, RAMBO, or 34.5ENVE. **Figure 5a** shows that PBS-treated tumors grew rapidly and animals had to be sacrificed by day 17 due to

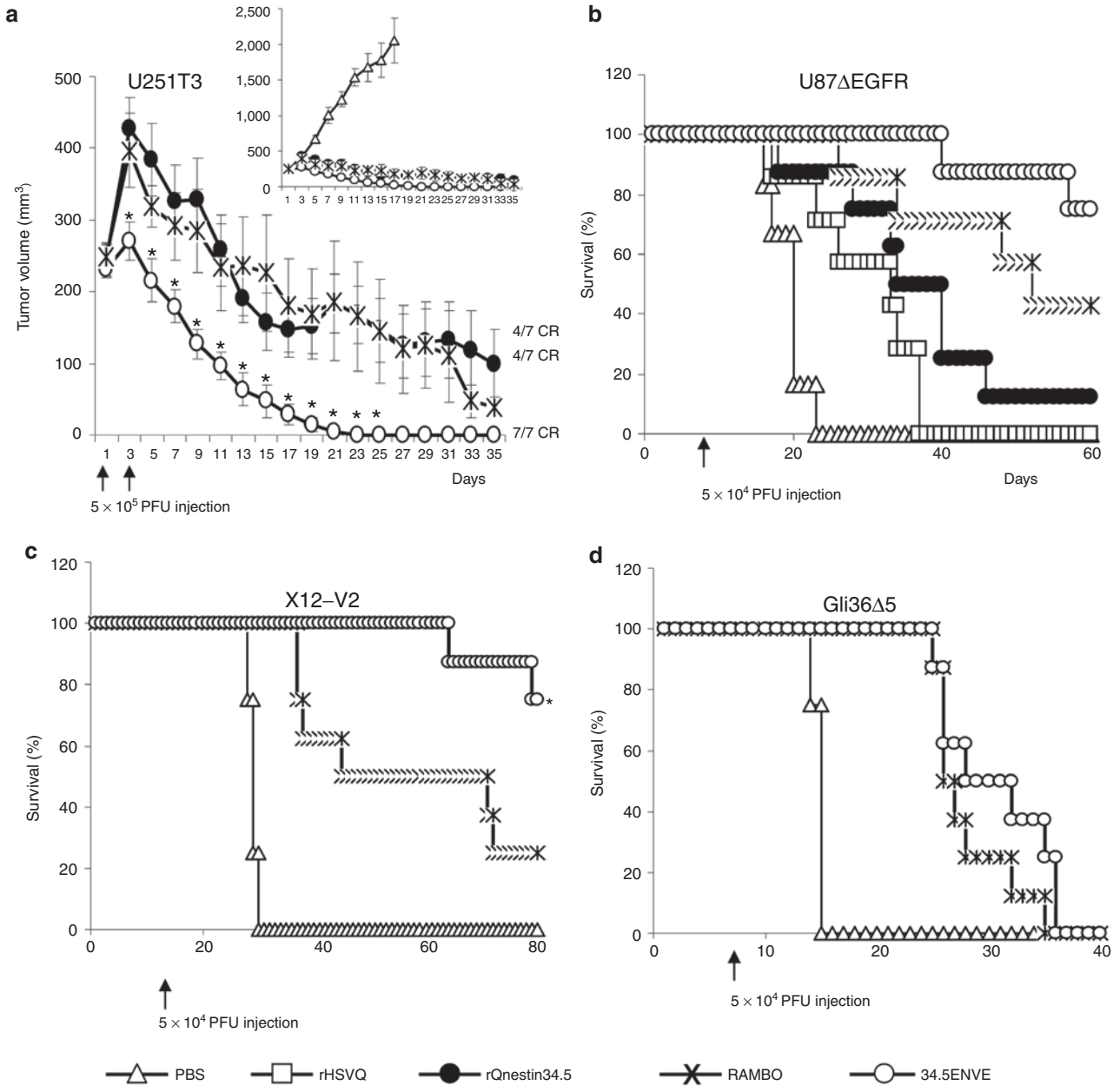

Figure 5 Antitumor effects of 34.5ENVE *in vivo*. (**a**) Antitumor efficacy of 34.5ENVE against U251T3 subcutaneous glioma model. Mice with U251T3 subcutaneous tumors were treated with phosphate-buffered saline (PBS) or 5 × 10^5 plaque-forming unit (pfu) every other day for a total of two times (Q2Dx2) once tumors reached an average volume of 250 mm^3. Mean tumor growth of mice after treatment with PBS, rQnestin34.5, RAMBO, or 34.5ENVE is shown as a function of time. CR: complete response shown in mice by day 49. (**b**) Kaplan–Meier survival curve of mice implanted with U87ΔEGFR intracranial glioma treated with PBS or 5 × 10^4 pfu of rHSVQ1, rQnestin34.5, RAMBO, or 34.5ENVE 7 days after tumor cell implantation. (**c**) Kaplan–Meier survival curve of mice implanted with X12-V2 intracranial glioma treated with PBS or 5 × 10^4 pfu of RAMBO or 34.5ENVE 10 days after tumor cell implantation. (**d**) Kaplan–Meier survival curve of mice implanted with Gli36Δ5 intracranial glioma treated with PBS or 5 × 10^4 pfu of RAMBO or 34.5ENVE 7 days after tumor cell implantation.

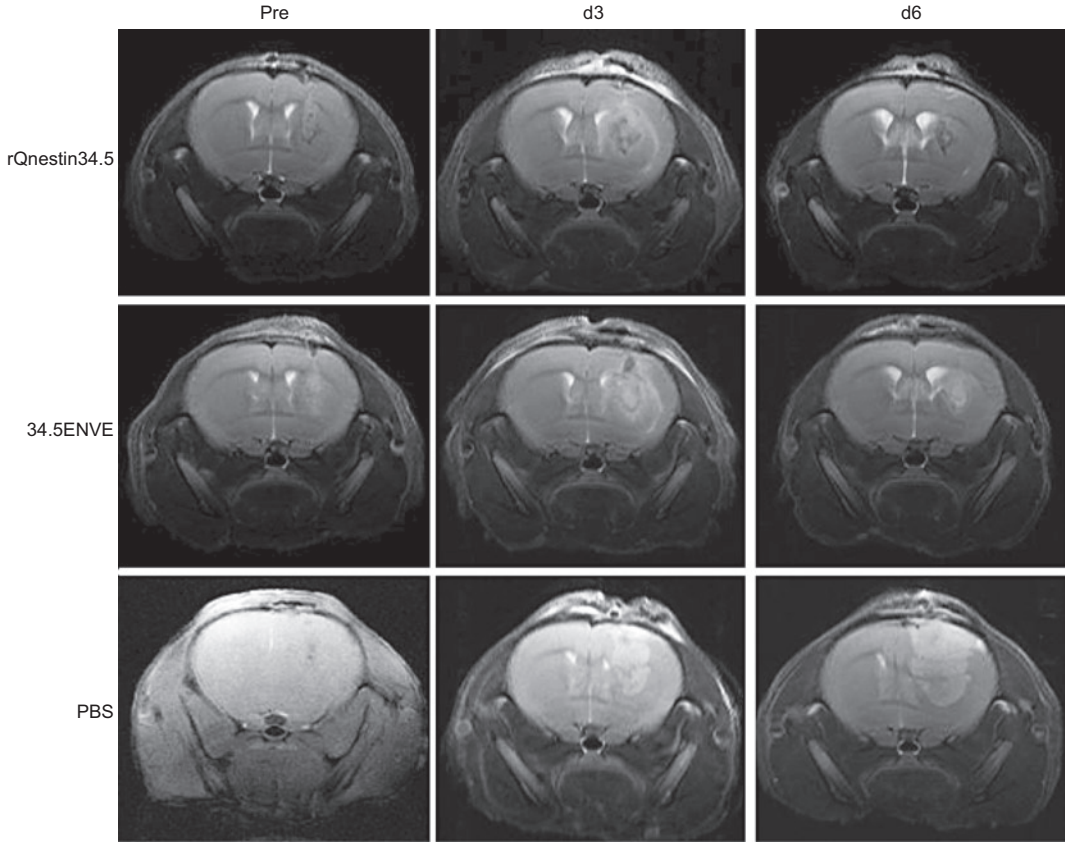

Figure 6 Oncolytic virus (OV) treatment induced tumor regression. T2-weighted MRI images of coronal sections of a representative tumor-bearing mouse 1 day before (left panel), 3 days after (middle panel), and 6 days after (right panel) treatment with rQnestin34.5 (top), 34.5ENVE (middle), or phosphate-buffered saline (PBS) (bottom).

tumor burden. In marked contrast, 7/7 mice treated with 34.5ENVE showed complete tumor regression by day 25, whereas on a long-term follow-up to day 49, only 4/7 mice treated with RAMBO or rQnestin34.5 showed a complete response with the rest of the mice showing progressive disease (as measured by increasing tumor volume). We next compared the antitumor efficacy of 34.5ENVE in mice bearing an intracranial U87ΔEGFR (**Figure 5b**), X12-V2 (**Figure 5c**), and Gli36Δ5 (**Figure 5d**) glioma. **Figure 5b** shows Kaplan–Meier curves for survival of mice (with U87ΔEGFR glioma) in each group (n = 8/group). Control mice treated with PBS died of tumor burden (median survival: 20 days), whereas mice treated with rHSVQ1, rQnestin34.5, RAMBO, or 34.5ENVE showed increased median survivals (median survival = 33, 34, 53, and >80 days, respectively). Consistent with our previous results, mice treated with RAMBO showed a significant increase in median survival compared to rHSVQ1-treated mice.[5] Significantly, 75% of the mice treated with 34.5ENVE lived longer than 80 days at which point they were sacrificed and found to be tumor free (P < 0.001 between 34.5ENVE and rHSVQ1, P = 0.002 between 34.5ENVE and rQnestin 34.5, P = 0.077 between 34.5ENVE and RAMBO). To evaluate whether antitumor efficacy of 34.5ENVE was dependent on nestin status of cells, we compared antitumor efficacy of 34.5ENVE and RAMBO in glioma with high (X12-V2) and low nestin (Gli36Δ5) expression (**Supplementary Figure S1**). Consistent with nestin driven specificity of 34.5ENVE, we observed a significant increase in antitumor efficacy of 34.5ENVE compared to RAMBO in high nestin-expressing X12-V2 intracranial glioma-bearing mice (P = 0.026 between RAMBO and 34.5ENVE) with no difference in low nestin-expressing Gli36Δ5 glioma-bearing mice (**Figure 5c,d**).

Increased necrosis in tumors treated with 34.5ENVE

In a parallel experiment to measure the impact of Vstat120 expressed by 34.5ENVE on the tumor microenvironment, we used dynamic contrast-enhanced MRI (DCE-MRI) to noninvasively measure the antitumor response to rQnestin34.5 and 34.5ENVE treatment in intracranial glioma (U87ΔEGFR) bearing mice. Mice were treated with PBS (n = 3/group), rQnestin34.5 (n = 4/group), or 34.5ENVE (n = 4/group) on day 10 post-tumor cell implantation. **Figure 6** shows representative coronal T2-weighted MRI images from one mouse/group pretreatment and on days 3 and 6 post-treatment, respectively. Assessment of tumor volumes in all mice showed that while PBS-treated tumors grew rapidly, all of the OV-treated tumors showed initial increase in apparent tumor volume (comparing day 3 post-treatment to pretreatment), followed by tumor regression on day 6 post-treatment. Interestingly, despite a better survival, we did not observe a significant difference in tumor volume shrinkage measured by T2-weighted MRI between rQnestin34.5 and 34.5ENVE at these time points. Because tumoral necrosis and edema can contribute to apparent tumoral volume, we investigated changes in tumoral perfusion and necrosis in animals

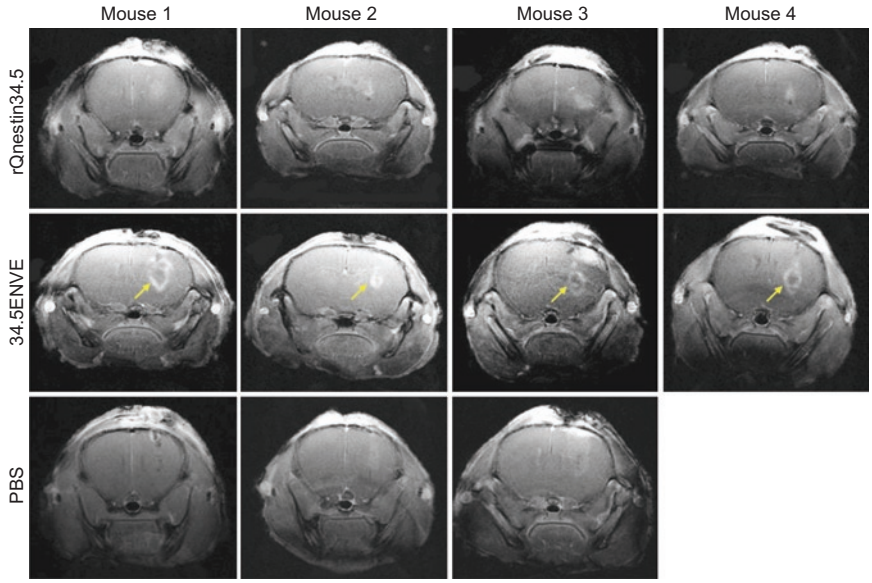

Figure 7 Contrast enhancement of phosphate-buffered saline (PBS) and oncolytic virus (OV)-treated tumors. Contrast-enhanced images of coronal sections of mice 3 days after treatment with PBS (n = 3), rQnestin34.5 (n = 4), or 34.5ENVE (n = 4). Diffusion of the contrast agent immediately after Gd-DTPA administration results in contrast enhancement appearing as area of high signal intensity. Arrow indicates the central nonenhancing core observed in all four of the mice treated with 34.5ENVE, which is not evident in any mice treated with rQnestin34.5 or PBS.

treated with rQnestin34.5 and 34.5ENVE. **Figure 7** shows contrast enhancement of all tumor-bearing mice imaged 3 days after the indicated treatment immediately following gadolinium diethylene-triamine penta-acetic acid (Gd-DTPA) administration. Contrast enhancement was evident in all of the OV-treated animals at the site of OV injection. However, in the 34.5ENVE-treated animals immediately after Gd-DTPA administration, there was a central unperfused area (yellow arrow) at the site of virus injection accompanied by increased leakiness surrounding this core (**Figure 7**), giving the appearance of a halo. We used Gd-DTPA-based DCE-MRI to calculate changes in K^{trans} and v_e between rQnestin34.5- and 34.5ENVE-treated animals (**Supplementary Figure S2**). K^{trans} refers to increased leakage of contrast agent and suggests increased endothelial permeability facilitating the entry of the contrast agent from the blood plasma, and v_e refers to the volume of contrast in the extravascular and extracellular space per unit volume of tissue.[15] We found a significant increase in v_e, in animals treated with 34.5ENVE compared to rQnestin34.5, (P = 0.0009, n = 4/group) without a significant change in K^{trans} (**Supplementary Figure S2**). Spatially, the increased v_e in all the 34.5ENVE-treated animals was localized to the noncontrast enhancing core visualized immediately after Gd-DTPA administration (**Figure 8a**). Such a pattern of increase of v_e in the noncontrast enhancing area has been shown to indicate tumoral necrosis.[16] We thus investigated the noncontrast enhancing core further using histological analysis. **Figure 8b** shows representative hematoxylin and eosin stained images of tumor-bearing brain sections, showing increased necrosis (asterisks) in the intracranial tumor core of animals treated with 34.5ENVE compared to rQnestin34.5. Collectively, these findings indicate that 34.5ENVE treatment results in increased tumor necrosis and enhanced antitumor efficacy compared to rQnestin34.5.[16]

DISCUSSION

OV treatment is a promising biological therapy currently being evaluated in human patients for safety and efficacy. Rapid viral clearance along with reduced viral replication in tumor cells is thought to be one of the major factors responsible for limited efficacy.[17] Transcriptional retargeting of OV by utilizing glioma-specific nestin enhancer driven ICP34.5 expression has been described and has shown efficacy in preclinical models of glioma and neuroblastoma.[9–11] Nestin was initially described as a marker for neuronal stem cells, however, its expression has been reported in several malignancies including brain, gastrointestinal, pancreatic, prostate, breast, malignant melanoma, and thyroid tumors.[18] Thus, nestin driven OVs have therapeutic significance for many different types of cancer.[9–11] Apart from virus replication, the tumor microenvironment also presents a formidable barrier for OV therapy, and arming of OV with antiangiogenic genes has shown promise in several preclinical studies.[19] Here, we describe the construction and antitumor efficacy of 34.5ENVE, an OV transcriptionally driven to have increased virus replication in nestin-positive tumor cells and armed with the antiangiogenic *Vstat120* gene to modulate the tumor microenvironment.

Vstat120 is an extracellular fragment of brain angiogenesis inhibitor 1, whose expression has been shown to be reduced in several malignancies.[20–24] Given the antiangiogenic role attributed to Vstat120, the reconstitution of its expression in brain angiogenesis inhibitor 1 null tumors may enhance anticancer therapeutic efficacy.[5,25–28] The antiangiogenic effects of Vstat120 are attributed to five thrombospondin type 1 domains within its N terminal sequence, and an integrin antagonizing RGD motif.[27–29] Oncolytic HSV-1 therapy has been shown to reduce TSP-1 protein, and also increase integrin-activating CCN1 protein in the tumor extracellular matrix, resulting in an increased

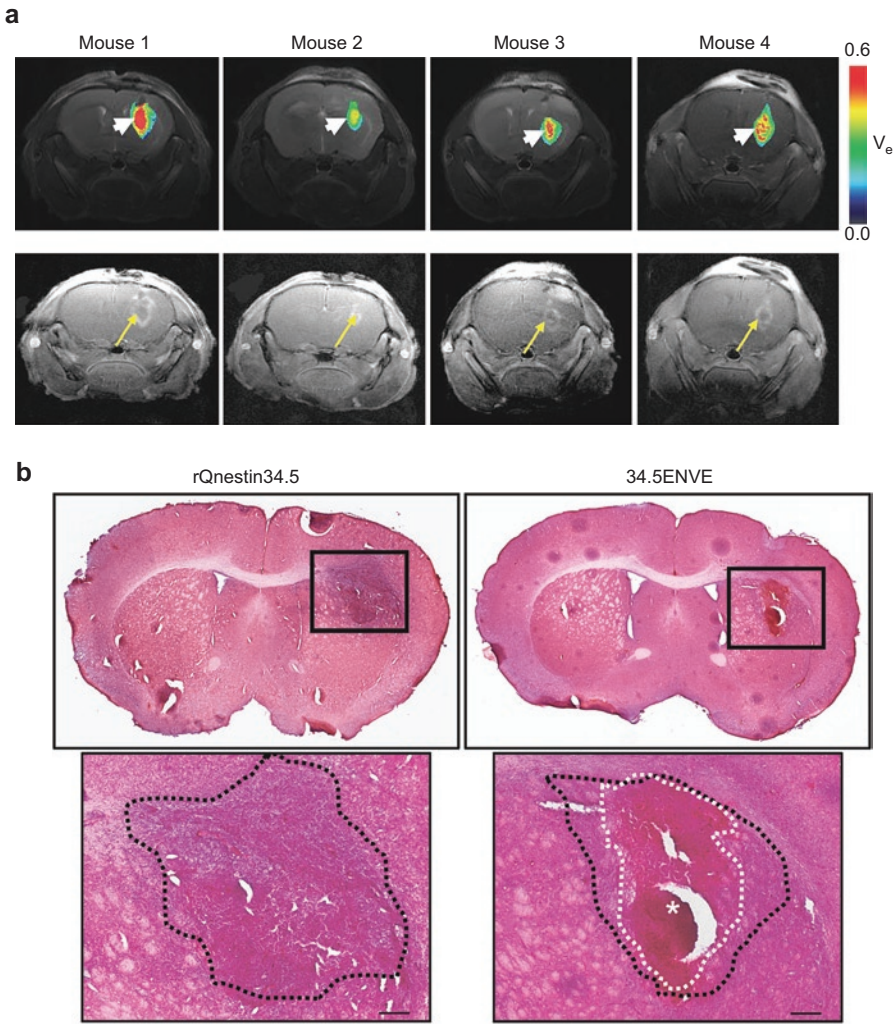

Figure 8 Effect of 34.5ENVE on tumor necrosis. (**a**) Inverse spatial correlation of v_e and contrast enhancing tumor area in 34.5ENVE-treated mice. Color-coded parametric images of v_e in each of the four 34.5ENVE treated mice 3 days post-treatment (top) show increased v_e (arrow head) in tumoral area that initially lacked contrast enhancement (arrow) immediately after Gd-DTPA administration in each of the four mice treated with 34.5ENVE. (**b**) Histologic analysis of necrosis in rQnestin34.5- and 34.5ENVE-treated brain tumors. In a parallel study, the above experiment was repeated and animals were sacrificed 3 days post-treatment for histological analysis of tumor-bearing brain. Representative hematoxylin and eosin (H&E) stained sections of rQnestin34.5- and 34.5ENVE-treated animals. Large necrotic area evident in 34.5ENVE-treated tumor (white dotted line and asterisks) is surrounded by viable tumor area (black dotted line). Bar = 200 µm.

angiogenesis in the residual tumors after OV therapy.[30,31] Thus, we hypothesized that Vstat120 gene delivery in conjunction with transcriptionally retargeted oncolysis would reduce OV induced vascular permeability and prolong OV propagation and efficacy in tumors.

Here, we describe significant antitumor efficacy of 34.5ENVE in both subcutaneous and intracranial glioma models. Changes in vascular permeability have been correlated with both increased and reduced OV efficacy.[32,33] Here, we used DCE-MRI of mice with intracranial tumors to investigate the impact of Vstat120 on vessel leakiness. Whereas there was no change in absolute value of K^{trans} between rQnestin34.5 and 34.5ENVE, analysis of the parametric images of v_e along with histologic analysis of intracranial tumors showed increased tumoral necrosis in 34.5ENVE-treated animals. Future studies evaluating its safety and biodistribution in HSV-1 sensitive BalbC mice will be needed before its clinical investigation in patients.

In conclusion, this study reports on the construction and antitumor efficacy of a novel, transcriptionally driven OV with unsurpassed antitumor efficacy and encourages its further development as a potent therapeutic agent for patients.

MATERIALS AND METHODS

Cell lines and viruses. Human normal astrocytes, hepatocytes, human umbilical vein endothelial cells, and HDMEC were purchased from ScienCell (Sandiego, CA). Vero cells were obtained from ATCC (Manassas, VA). U251, LN229, T98G, Gli36Δ5, have been cultured in our laboratory and U251T3 cells were obtained as a tumorigenic clone of U251 cells by serially passaging these cells three times in mice. U87ΔEGFR cell line expresses a truncated, constitutively active, mutant form of epidermal growth factor receptor (EGFRvIII), and has been previously described.[34] X12 primary tumor derived cells were obtained from Dr Sarkaria, and were subcloned to express green fluorescent protein to generate X12-V2 (Mayo Clinic, Rochester, MN).[30] All the cells were evaluated for their nestin expression by reverse transcriptase-PCR as described (**Supplementary Figure S1**).[9]

The construction and efficacy of RAMBO, a Vstat120-expressing OV within the context of rHSVQ1, a first generation OV deleted for both copies of ICP34.5 and disrupted for ICP6, and rQnestin34.5, a transcriptionally driven OV-expressing ICP34.5 under the control of glioma-specific nestin promotor, have been previously described.[5,9] To generate 34.5ENVE, the expression cassette encoding for *Vstat120* gene under the control of the viral IE4/5 promotor and ICP34.5 under the regulation of nestin enhancer driven promotor was inserted into fHSVQ using HSVQuik technology as previously described.[12] All viruses were propagated in Vero cells. Three days after infection, secreted virus and virus-infected Vero cells were harvested and subjected to three cycles of freeze-thaw to release the viruses completely, and cell debris was cleared by centrifugation (4,000*g*, 20 minutes). Virus was filtered to remove cell debris and pelleted by centrifugation at 13,000*g* for 1 hours. The titer (plaque-forming units (pfu)/ml) of the resulting virus was determined by pfu assay in Vero cells.[12]

Cell viability and virus replication assays. To measure OV-mediated cytotoxicity in 96-well plates, cells were infected with the indicated virus at the indicated multiplicity of infection. Seventy-two hours after infection, viable cells were measured by a standard crystal violet assay as described.[5] For virus replication assays, the indicated glioma cells were infected at an multiplicity of infection of 0.01 for 2 hours, washed and media replaced. Three days following infection, cells and supernatant were harvested and the number of infectious virus particles present was determined by performing a standard pfu assay on Vero cells.

In vitro endothelial cell assays. U251 glioma cells were infected with the indicated virus at an multiplicity of infection of 2. After 14 hours, CM was harvested and cellular debris and free-floating virions were removed by centrifugation (27,700*g* for 1 hour). The CM was then concentrated 100-fold in Amicon Ultra centrifuge tubes (Millipore, Billerica, MA), and 0.4% of immunoglobulin G was added to neutralize contaminated OV. Endothelial cell migration assays were performed using transwell chambers (8-μm pore size, from Corning Costar (Cambridge, MA) coated with 0.1% fibronectin as previously described.[5] Tube formation assay was performed as described previously.[35] Briefly, HDMECs were grown on growth factor-reduced Matrigel (Collaborative Biomedical Products, Bedford, MA). Cells were then allowed to form tubes for 4 hours at 37 °C, and photographed (×200). Pictures of the formed tubes (200 μm or larger, and connected at both ends) were quantified by counting 10 microscopic view/well, and the data presented as the averages of four wells.

Antibodies. For western blot analysis: anti-brain angiogenesis inhibitor 1 antibodies were raised as described previously,[26] antihuman GAPDH (ab9484) and anti-ICP4 (ab6514) were purchased from Abcam (Cambridge, MA), and anti-eIF2α (9722) and anti-phosphor-eIF2α (9721) were obtained from Cell Signaling Technology (Beverly, MA). To observe MVD, tumor sections were treated with purified rat anti-mouse CD31 (Pharmingen, San Jose, CA) to visualize endothelial cells lining the blood vessels (n = 3 mice/group), and then with biotin-conjugated goat anti-rat immunoglobulin G (BD Biosciences Pharmingen, San Diego, CA). The three most vascularized areas within the tumor ("hot spots") were chosen at low magnification, and vessels were counted under a representative high-magnification (×200) field in each view field.[36] Mean MVD was calculated as the average of counts/view field in three hot spot areas as described by Dr Folkman.[14] Vessels at the periphery of the tumor were disregarded in the MVD counts. The MVD for each group was then averaged together (n = 2–4 sections/tumor, and n = 3 tumors/group) to get the final count ± SEM.

Animal surgery. All animal experiments were performed in accordance with the Subcommittee on Research Animal Care of The Ohio State University guidelines and have been approved by the institutional review board. Six- to eight-week-old Female athymic nu/nu mice (Charles River Laboratories, Frederick, MD), were used for all tumor studies.

For subcutaneous tumors, nude mice were implanted with 1.5×10^7 U251T3 glioma cells into the rear flank. When tumors reached an average size of 250 mm^3, mice were administered PBS, or the indicated virus by direct intratumoral injection (5×10^5 pfu) on days 1 and 3. Tumor volume was calculated using the following formula: volume = 0.5 LW^2 as described.[37]

For intracranial tumor studies, anesthetized nude mice were fixed in a stereotactic apparatus, and a burr hole was drilled at 2-mm lateral to the bregma, to a depth of 3 mm. U87ΔEGFR (1×10^5), X12-V2 (3×10^5), or Gli36Δ5 (1×10^5) glioma cells were implanted. On day 7, 10, and 7 after U87ΔEGFR, X12-V2 or Gli36Δ5 glioma cell implantation, respectively, the mice were anesthetized again and stereotactically inoculated with 5×10^4 pfu of the indicated virus at the same location. Animals were observed daily and were euthanized at the indicated time points or when they showed signs of morbidity.

DCE-MRI imaging. Mice-bearing intracranial tumors were treated with PBS or the indicated virus on day 10 after tumor cell implantation. Anatomic imaging was done on day 9 (pretreatment), on day 13 (3 days post-treatment), and on day 16 (6 days post-treatment), using T2-weighted RARE imaging sequence (TR = 2,500 ms, TE = 12 ms, rare factor = 8, navgs = 4). The imaging was performed using a Bruker Biospin 94/30 magnet (Bruker Biospin, Karlsruhe Germany). For dynamic contrast-enhanced imaging (DCE-MRI), anaesthetized mice were injected with 0.5 mmol/kg Magnevist (Bayer Health Care Pharmaceuticals, Wayne, NJ) Gd-DTPA contrast agent. A 2.0-cm diameter receive-only mouse brain coil was placed over the head, and the mouse bed with surface coil was placed inside a 70-mm diameter linear volume coil. DCE data were collected using a FLASH sequence (TR = 135.8 ms, TE = 2.4, flip angle = 50°). Several baseline images were collected before the bolus of Gd-DTPA was injected through the tail vein catheter. Images were collected after Gd-DTPA injection for ~30 minutes. The acquisition parameters for both the T1- and T2-weighted multislice scans were as follows: FOV = 20 mm × 20 mm, slice thickness = 1.0 mm, matrix size = 256 × 256.

For data analysis, a region-of-interest (ROI) that included the tumor was manually outlined using the T2-weighted images. Tumor volumes were calculated from the outlined ROI. Gd-DTPA concentrations were measured for all voxels within the ROI using the method described.[38] A fixed value of T1(0) was chosen as 2,029 based on T1 measurements made in normal mouse brain at 9.4T.[39] $C(t)$ was calculated for each voxel within the ROI and the average for the entire ROI was calculated. The integrated area under the curve (IAUC) was calculated from the mean Gd-DTPA $C(t)$ curve postinjection and the cumulative IAUC (CIAUC) was calculated from the IAUC. The mean $C(t)$, IAUC, and CIAUC curves were evaluated and compared for the rQnestin34.5, 34.5ENVE, and PBS-treated mice at each imaging time point. The vascular input function required for the pharmokinetic modeling was obtained by measuring signal intensity in the superficial temporal vein within the same image slices as those of the tumor. A two-compartment general kinetic model was used for analyzing the distribution and flow of gadolinium in the tumor. The rate constant, K^{trans}, and the extravascular exctracellular space, v_e, were determined by nonlinear curve fitting the Gd concentration, $C(t)$, over a 20-minute time period after Gd injection. Color-coded maps for K^{trans} and v_e were created to visualize the spatial distribution of Gd in the tumor. Histograms of K^{trans} and v_e for the entire tumors were calculated and median values were compared between the treatment groups.

Statistical analysis. Student's t-test was used to analyze changes in cell killing, HDMEC transwell migration, tube formation assay data, and changes in MVD. A $P < 0.05$ was considered statistically significant. In the survival analysis, Kaplan–Meier curves were plotted and compared using the log rank test. Spearman's rank correlation coefficient was calculated and compared for the correlation analysis on the fold change (Log2) in virus replication of rQnestin34.5/34.5ENVE compared to rHSVQ1. Holm's procedure was used to correct the P value for multiple comparisons. A $P < 0.05$ was

considered statistically significant. All statistical analyses were performed with the use of SPSS statistical software (version 14.0; SPSS, Chicago, IL), or SAS (version 9.2; SAS Institute, Cary, NC).

SUPPLEMENTARY MATERIAL

Figure S1. RT-PCR analysis of the indicated glioma cell lines for relative nestin expression.

Figure S2. (**a**–**d**) Color-coded parametric images K^{trans} (**a**–**b**) and v_e (**c**–**d**) of coronal sections of mice 3 days after treatment with rQnestin34.5 (**a**, **c**), or 34.5ENVE (**b**, **d**).

ACKNOWLEDGMENTS

This work was supported by funding from the National Institutes of Health grant (1R01NS064607, and 1R01CA150153 to B.K.; NS045758 to C.B.) and the National Research Foundation of Korea Grant funded by the Korean Government (NRF-2009-352-E00035 to J.Y.Y).

REFERENCES

1. Stupp, R, Mason, WP, van den Bent, MJ, Weller, M, Fisher, B, Taphoorn, MJ *et al.*; European Organisation for Research and Treatment of Cancer Brain Tumor and Radiotherapy Groups; National Cancer Institute of Canada Clinical Trials Group. (2005). Radiotherapy plus concomitant and adjuvant temozolomide for glioblastoma. *N Engl J Med* **352**: 987–996.
2. Markert, JM, Liechty, PG, Wang, W, Gaston, S, Braz, E, Karrasch, M *et al.* (2009). Phase Ib trial of mutant herpes simplex virus G207 inoculated pre-and post-tumor resection for recurrent GBM. *Mol Ther* **17**: 199–207.
3. Markert, JM, Medlock, MD, Rabkin, SD, Gillespie, GY, Todo, T, Hunter, WD *et al.* (2000). Conditionally replicating herpes simplex virus mutant, G207 for the treatment of malignant glioma: results of a phase I trial. *Gene Ther* **7**: 867–874.
4. Post, DE, Khuri, FR, Simons, JW, Van Meir, EG (2003). Replicative oncolytic adenoviruses in multimodal cancer regimens. *Hum Gene Ther* **14**: 933–946.
5. Hardcastle, J, Kurozumi, K, Dmitrieva, N, Sayers, MP, Ahmad, S, Waterman, P *et al.* (2010). Enhanced antitumor efficacy of vasculostatin (Vstat120) expressing oncolytic HSV-1. *Mol Ther* **18**: 285–294.
6. Prabhakar, S, Messerli, SM, Stemmer-Rachamimov, AO, Liu, TC, Rabkin, S, Martuza, R *et al.* (2007). Treatment of implantable NF2 schwannoma tumor models with oncolytic herpes simplex virus G47Delta. *Cancer Gene Ther* **14**: 460–467.
7. Hardcastle, J, Kurozumi, K, Chiocca, EA and Kaur, B (2007). Oncolytic viruses driven by tumor-specific promoters. *Curr Cancer Drug Targets* **7**: 181–189.
8. Wojton, J and Kaur, B (2010). Impact of tumor microenvironment on oncolytic viral therapy. *Cytokine Growth Factor Rev* **21**: 127–134.
9. Kambara, H, Okano, H, Chiocca, EA and Saeki, Y (2005). An oncolytic HSV-1 mutant expressing ICP34.5 under control of a nestin promoter increases survival of animals even when symptomatic from a brain tumor. *Cancer Res* **65**: 2832–2839.
10. Kambara, H, Saeki, Y and Chiocca, EA (2005). Cyclophosphamide allows for *in vivo* dose reduction of a potent oncolytic virus. *Cancer Res* **65**: 11255–11258.
11. Mahller, YY, Williams, JP, Baird, WH, Mitton, B, Grossheim, J, Saeki, Y *et al.* (2009). Neuroblastoma cell lines contain pluripotent tumor initiating cells that are susceptible to a targeted oncolytic virus. *PLoS ONE* **4**: e4235.
12. Terada, K, Wakimoto, H, Tyminski, E, Chiocca, EA and Saeki, Y (2006). Development of a rapid method to generate multiple oncolytic HSV vectors and their *in vivo* evaluation using syngeneic mouse tumor models. *Gene Ther* **13**: 705–714.
13. Chou, J, Chen, JJ, Gross, M and Roizman, B (1995). Association of a M® 90,000 phosphoprotein with protein kinase PKR in cells exhibiting enhanced phosphorylation of translation initiation factor eIF-2α and premature shutoff of protein synthesis after infection with gamma 134.5- mutants of herpes simplex virus 1. *Proc Natl Acad Sci USA* **92**: 10516–10520.
14. Weidner, N, Semple, JP, Welch, WR and Folkman, J (1991). Tumor angiogenesis and metastasis–correlation in invasive breast carcinoma. *N Engl J Med* **324**: 1–8.
15. Kerwin, WS, O'Brien, KD, Ferguson, MS, Polissar, N, Hatsukami, TS and Yuan, C (2006). Inflammation in carotid atherosclerotic plaque: a dynamic contrast-enhanced MR imaging study. *Radiology* **241**: 459–468.
16. Egeland, TA, Gaustad, JV, Galappathi, K and Rofstad, EK (2011). Magnetic resonance imaging of tumor necrosis. *Acta Oncol* **50**: 427–434.
17. Friedman, A, Tian, JP, Fulci, G, Chiocca, EA and Wang, J (2006). Glioma virotherapy: effects of innate immune suppression and increased viral replication capacity. *Cancer Res* **66**: 2314–2319.
18. Ishiwata, T, Matsuda, Y and Naito, Z (2011). Nestin in gastrointestinal and other cancers: effects on cells and tumor angiogenesis. *World J Gastroenterol* **17**: 409–418.
19. Kaur, B, Cripe, TP and Chiocca, EA (2009). "Buy one get one free": armed viruses for the treatment of cancer cells and their microenvironment. *Curr Gene Ther* **9**: 341–355.
20. Kaur, B, Brat, DJ, Calkins, CC and Van Meir, EG (2003). Brain angiogenesis inhibitor 1 is differentially expressed in normal brain and glioblastoma independently of p53 expression. *Am J Pathol* **162**: 19–27.
21. Nishimori, H, Shiratsuchi, T, Urano, T, Kimura, Y, Kiyono, K, Tatsumi, K *et al.* (1997). A novel brain-specific p53-target gene, BAI1, containing thrombospondin type 1 repeats inhibits experimental angiogenesis. *Oncogene* **15**: 2145–2150.
22. Fukushima, Y, Oshika, Y, Tsuchida, T, Tokunaga, T, Hatanaka, H, Kijima, H *et al.* (1998). Brain-specific angiogenesis inhibitor 1 expression is inversely correlated with vascularity and distant metastasis of colorectal cancer. *Int J Oncol* **13**: 967–970.
23. Hatanaka, H, Oshika, Y, Abe, Y, Yoshida, Y, Hashimoto, T, Handa, A *et al.* (2000). Vascularization is decreased in pulmonary adenocarcinoma expressing brain-specific angiogenesis inhibitor 1 (BAI1). *Int J Mol Med* **5**: 181–183.
24. Lee, JH, Koh, JT, Shin, BA, Ahn, KY, Roh, JH, Kim, YJ *et al.* (2001). Comparative study of angiostatic and anti-invasive gene expressions as prognostic factors in gastric cancer. *Int J Oncol* **18**: 355–361.
25. Kudo, S, Konda, R, Obara, W, Kudo, D, Tani, K, Nakamura, Y *et al.* (2007). Inhibition of tumor growth through suppression of angiogenesis by brain-specific angiogenesis inhibitor 1 gene transfer in murine renal cell carcinoma. *Oncol Rep* **18**: 785–791.
26. Kaur, B, Brat, DJ, Devi, NS and Van Meir, EG (2005). Vasculostatin, a proteolytic fragment of brain angiogenesis inhibitor 1, is an antiangiogenic and antitumorigenic factor. *Oncogene* **24**: 3632–3642.
27. Kaur, B, Cork, SM, Sandberg, EM, Devi, NS, Zhang, Z, Klenotic, PA *et al.* (2009). Vasculostatin inhibits intracranial glioma growth and negatively regulates *in vivo* angiogenesis through a CD36-dependent mechanism. *Cancer Res* **69**: 1212–1220.
28. Klenotic, PA, Huang, P, Palomo, J, Kaur, B, Van Meir, EG, Vogelbaum, MA *et al.* (2010). Histidine-rich glycoprotein modulates the anti-angiogenic effects of vasculostatin. *Am J Pathol* **176**: 2039–2050.
29. Koh, JT, Kook, H, Kee, HJ, Seo, YW, Jeong, BC, Lee, JH *et al.* (2004). Extracellular fragment of brain-specific angiogenesis inhibitor 1 suppresses endothelial cell proliferation by blocking $\alpha v\beta 5$ integrin. *Exp Cell Res* **294**: 172–184.
30. Kurozumi, K, Hardcastle, J, Thakur, R, Shroll, J, Nowicki, M, Otsuki, A *et al.* (2008). Oncolytic HSV-1 infection of tumors induces angiogenesis and upregulates CYR61. *Mol Ther* **16**: 1382–1391.
31. Aghi, M, Rabkin, SD and Martuza, RL (2007). Angiogenic response caused by oncolytic herpes simplex virus-induced reduced thrombospondin expression can be prevented by specific viral mutations or by administering a thrombospondin-derived peptide. *Cancer Res* **67**: 440–444.
32. Kurozumi, K, Hardcastle, J, Thakur, R, Yang, M, Christoforidis, G, Fulci, G *et al.* (2007). Effect of tumor microenvironment modulation on the efficacy of oncolytic virus therapy. *J Natl Cancer Inst* **99**: 1768–1781.
33. Breitbach, CJ, Paterson, JM, Lemay, CG, Falls, TJ, McGuire, A, Parato, KA *et al.* (2007). Targeted inflammation during oncolytic virus therapy severely compromises tumor blood flow. *Mol Ther* **15**: 1686–1693.
34. Narita, Y, Nagane, M, Mishima, K, Huang, HJ, Furnari, FB and Cavenee, WK (2002). Mutant epidermal growth factor receptor signaling down-regulates p27 through activation of the phosphatidylinositol 3-kinase/Akt pathway in glioblastomas. *Cancer Res* **62**: 6764–6769.
35. Yoo, JY, Kim, JH, Kwon, YG, Kim, EC, Kim, NK, Choi, HJ *et al.* (2007). VEGF-specific short hairpin RNA-expressing oncolytic adenovirus elicits potent inhibition of angiogenesis and tumor growth. *Mol Ther* **15**: 295–302.
36. Choi, WW, Lewis, MM, Lawson, D, Yin-Goen, Q, Birdsong, GG, Cotsonis, GA *et al.* (2005). Angiogenic and lymphangiogenic microvessel density in breast carcinoma: correlation with clinicopathologic parameters and VEGF-family gene expression. *Mod Pathol* **18**: 143–152.
37. Yoo, JY, Kim, JH, Kim, J, Huang, JH, Zhang, SN, Kang, YA *et al.* (2008). Short hairpin RNA-expressing oncolytic adenovirus-mediated inhibition of IL-8: effects on antiangiogenesis and tumor growth inhibition. *Gene Ther* **15**: 635–651.
38. Haacke, EM, Filleti, CL, Gattu, R, Ciulla, C, Al-Bashir, A, Suryanarayanan, K *et al.* (2007). New algorithm for quantifying vascular changes in dynamic contrast-enhanced MRI independent of absolute T1 values. *Magn Reson Med* **58**: 463–472.
39. Kuo, YT, Herlihy, AH, So, PW, Bhakoo, KK and Bell, JD (2005). *In vivo* measurements of T1 relaxation times in mouse brain associated with different modes of systemic administration of manganese chloride. *J Magn Reson Imaging* **21**: 334–339.